Reactive extrusion of sol-gel silica as fire retardant synergistic additive in ethylene-vinyl acetate copolymer (EVA) composites

Reactive extrusion of sol-gel silica as fire retardant synergistic additive in Ethylene-Vinyl Acetate copolymer (EVA) composites

D. Battegazzore[a*], M. Lavaselli[a], B. Cheng[b], D. Li[b], R. Yang[b], A. Frache[a], G. Paul[c], L. Marchese[c]

[a]*Politecnico di Torino, Alessandria Site, V.le Teresa Michel 5, 15121 Alessandria (Italy) – daniele.battegazzore@polito.it*

[b]*Beijing Institute of Technology, South Zhongguancun Street 5, Haidian District, 100081 Beijing (China)*

[c]*Department of Sciences and Technological Innovation, University of Eastern Piedmont A. Avogadro, V.le Teresa Michel 11, 15121 Alessandria (Italy)*

Abstract

Silica derived from sol-gel approach was used as co-filler in aluminium hydroxide (ATH) or hydromagnesite (HM) ethylene-vinyl acetate (EVA) formulations. In this bottom-up approach, the silica network is formed inside the extruder in a first process step. The 3D silica structure is investigated by solid-state nuclear magnetic resonance (ssNMR) spectroscopy and a combined TGA-FTIR analysis revealing a partially incomplete reaction to form silica particles. In addition, ^{29}Si CPMAS NMR showed the formation of chemical Si-C bonds between EVA and silica networks. The performance enhancement of the fire retardant properties was established by comparing with composites prepared by a top-down approach, i.e by adding preformed silica. It is confirmed that the preformed silica acts as a synergistic agent with both ATH or HM, increasing the flame retardant properties (limiting oxygen index, UL-94 and cone calorimeter tests) of EVA

composites, however, the sol-gel silica shows the best performances in reducing both heat release and smoke production. The role of the sol-gel structure was deeply investigated in correlation with combustion test.

Keywords: Ethylene(vinyl acetate) copolymer; sol-gel silica; reactive extrusion; fire retardant properties; cone calorimetry; aluminium hydroxide; hydromagnesite; solid-state nuclear magnetic resonance; TGA-FTIR.

Introduction

Ethylene-vinyl acetate copolymer (EVA) is a widely used material. The primary applications are packaging film / co-extrusion layers, adhesives / paper coatings, wire and cable insulation, carpet backing, moulded or extruded items, foam and sound damping / sound barrier sheet [1]. EVA is highly flammable and emits a large amount of smoke during combustion thus it needs to be formulated with additives to provide a fire retardant behaviour required in many applications [2]. The traditional technique used for increasing the EVA flame retardancy was the addition of large quantities of inorganic filler, such as aluminium trihydroxide (ATH) or magnesium hydroxide (MH) [3] [4] [5] [6] [7]. These compounds act both in the condensed and the gas phase following endothermic decomposition with water/CO_2 release, which reduces the temperature of the material and of the surrounding gas phase and dilutes the fuel supply [8] [9]. The second major fire retardant mechanism provided by such kind of fillers is the barrier effect. Indeed, during the decomposition of the polymer, the mineral fillers accumulate on the surface where form a protective layer. This layer limits the supply of the flame with

degradation gases, and protects the underlying polymer from the heat flux [5, 10].

Unfortunately, some drawbacks are present in the use of such formulations. Firstly, a high amount of inorganic fillers is necessary to be efficient for fire retardancy (generally 60 wt.-%). This fact leads to a reduction of the mechanical properties and limits the material processability.

Many investigations have been done combining these hydroxides with other halogen-free flame retardant synergistic agents [3, 10-18] in order to enhance flame retardance and decrease the high loading level. One of the most used synergic co-filler is silica, which greatly reduces the heat release and mass loss rates and, at the same time, depresses the smoke release during the combustion. The inclusion of this co-filler was always studied by means of the top-down approach, i.e. by mixing the silica particles together with the fire retardants (FRs) in the extrusion process.

One possible alternative solution consists in the use of sol–gel reactions to synthesize inorganic fillers directly in the polymeric matrix starting from a liquid precursor, namely a bottom-up approach [19, 20]. If these reactions are performed during the processing inside the extruder, firstly a well dispersion in the matrix is expected, secondly some condensation reactions may happen with other active species of the compound, i.e. FRs or polymer.

The main problem related to this method consists in the sol-gel reaction time that is generally longer than the extrusion process. Indeed, it is usual for an extrusion process to have a polymer residence time of few minutes and this time could be slightly varied by changing the parameters of extrusion and the screw profile but not drastically increased. On the other hand, the sol-gel reaction time is reported to be longer: as an example, gelation of TEOS dissolved in ethanol was reduced from 1000 hours to 92 hours when

HCl was employed [19, 21].

In the literature, only few studies have dealt with the synthesis of inorganic fillers through sol–gel chemistry in a single processing step. Dou et al. [22] created *in situ* silica in a polypropylene matrix in a mini-extruder. The inorganic precursor was a polyethoxysilane synthesized for this purpose and water was incorporated via a nitrogen flow containing water vapours. A similar approach was used by Prebe et al. [23] to create polylactide(PLA)/silica from a polydiethoxysilane. PA66/silica and PA6/phosphorylated silica composites were obtained by extrusion in a few minutes thanks to the high temperature of processing (>220°C), the residual water in the polyamides (0.08%) and the particular catalytic effect of amine and polyamide [24]. The later example reports on the great potential of reactive extrusion to create nanocomposites in a single fast high-temperature step without polymer degradation. A variation on those previously presented methods, concerns the incorporation into the melt polymer of an inorganic precursor solutions in which the hydrolysis–condensation reactions are initiated. This approach has been described in several studies concerning PLA, PCL, PP and polyethylene-co-octene [25-29]. As for the EVA matrix, Bonnet et al. [30] cross-linked EVA with diethylphosphatoethyltriethoxysilane creating an hybrid material containing silicon and phosphorus. By this way, they obtained a heat release rate peak reduction of 35% at the cone calorimeter compared to neat EVA.

The work described in this article is focused on the same purpose of fire retardant properties improvement, but exploring the synergistic mechanism of sol-gel silica with ATH or HM in the EVA. During the reactive extrusion, the sol-gel solution reacts to form a 3D silica network. This network could have many reactive sites still available for possible further reactions. Solid-state NMR spectroscopy as well as thermogravimetric

analysis (TGA) coupled with infrared spectroscopy (FTIR) were used to investigate the degree of conversion from TEOS to silica.

Limiting oxygen index measurements (LOI), UL-94 tests and the cone calorimeter tests were employed to verify the effectiveness of the sol-gel approach with respect to the direct incorporation of preformed silica for fire retardancy.

Experimental Section

2.1 Materials.

The Ethylene-Vinyl Acetate copolymer (EVA) used was the Bycolene V5110J grade from BASF-YPC Company Limited, with a melt flow index of 2.3~3.1 g/10min (190 °C, 2.16 kg) and a vinyl acetate content of 18.5 wt.-%.

Aluminium trihydroxide (ATH) AITEMAG A140FD ground-milled grade was supplied by Jiangsu ATK flame retardant material Co. Ltd, with an average diameter of 1.8 μm.

Hydromagnesite, Hydrated Magnesium Carbonate (HM) mineral powder was supplied by Tibet LaXin Investment Holding Co.Ltd, with an average diameter of 4.8 μm.

Tetraethyl orthosilicate (TEOS), ethanol and water were purchased from Beijing Chemical Reagents Company, citric acid was purchased from Aladdin Industrial Corporation. All these products were used as received without further purification.

A commercial silica, hydrophilic fumed silica, AEROSIL 200 produced by EVONIK Industries / Germany, was used for preparing some samples as comparison.

2.2. Sol-gel preparation

200 g of TEOS was mixed with 69.45g of water (molar ratio 1:4). Water plays a

fundamental role in the reaction kinetics and consequently on the final material's morphology as well as on the speed of the hydrolysis–condensation reactions [20]. An optimal H_2O/TEOS value between 4 and 8 is reported to allow the shortest reaction time [21]. In this study, the quantity of water is set to the minimum of this range to minimize the amount of water introduced into the extruder. Subsequently, 50g of ethanol was added to the TEOS and water solution under stirring to prevent phase separation during the first hydrolysis steps. Indeed, water and alkoxysilanes are not miscible thus a solvent such as an alcohol is needed for homogenization [21]. Finally, to speed up the reaction, an acid pH was used. For this purpose, 2.69g of citric acid was added to the solution. The final solution obtained is maintained under stirring for 3h at room temperature to allow the formation of a pre-gel. The aging time was chosen to obtain a solution with a viscosity still drawable by a peristaltic pump. After the 3 h of stirring, the pre-gel solution is pumped inside the main hopper of the extruder simultaneously with the polymer pellets feed.

2.3. Processing

The final composite materials were obtained by two melt mixing steps. In the first step two master-batches were obtained: a) EVA with FR and b) EVA with silica. In the second process the two obtained master-batches were mixed together to get the final formulations. In all cases, the total final filler content was fixed at 60 wt.-%.

2.3.1. Step Ia: Melt mixing of EVA with FR (ATH or HM)

The composite processing is conducted in a twin screw extruder CTE35 from Coperion

Keya (NanJing)Machinery Co., Ltd, with a screw diameter of 35mm and L/D ratio of 40. EVA-based composites were melt blended by direct feeding to the main hopper of the extruder with polymer and FR. The screw speed was fixed at 100 rpm. The heating temperature was set from 150 to 165°C into the five thermo-stated barrel blocks (as reported in Figure 1). One volumetric feeder was used for the feeding of a mechanically premixed polymer and powders. Close to screw end, a degassing hole in the barrel connected to a vacuum pump was present. The composite materials processed in the extruder are cooled in a water bath and pelletised. The total extrusion flow rate was fixed at 3 kg/h. The used screw profile is reported in Figure 1.

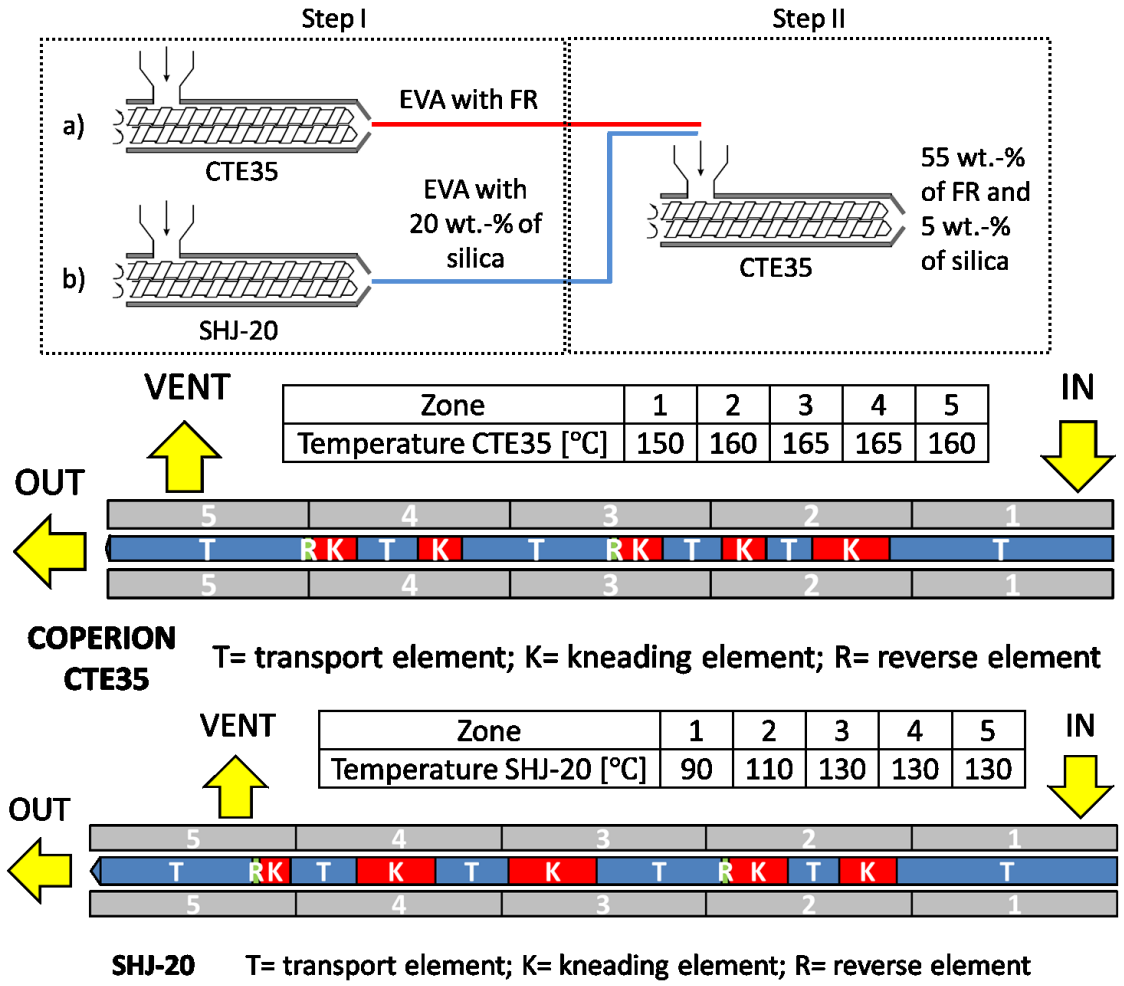

Figure 1. Screw and temperature profiles for the extrusion processes used.

A conventional melting zone consisting of transport elements (T in Figure 1) is used to melt the EVA granules. To provide a suitable mixing of FRs and polymer melt as well as to reduce the size of filler agglomerates or large particles, five kneading elements (K in Figure 1) prior to the atmospheric/vacuum degassing are used. Moreover, two counter conveying mixing elements (reverse elements R in Figure 1) were put after kneading blocks to maximize the mixing between fillers and polymer.

2.3.2. Step Ib: Melt mixing of EVA with silica (top down or bottom up approach)

A second twin screw extruder is SHJ-20 from NanJing Giant Machinery Co., Ltd, with a screw diameter of 21.7 mm and L/D ratio of about 39 and screw profile reported in Figure 1 was employed for the sol-gel reactive extrusion or for the direct silica particles incorporation.

The EVA granules are fed to the main hopper through a gravimetric feeder together with the aged liquid inorganic premix precursor TEOS/ethanol/water/catalyst by the use of a peristaltic pump BT100-2J from Longer Precision Pump Co., Ltd. The EVA extrusion flow rate and the sol-gel precursor flow were fixed at 900 g/h and 530 g/h, respectively (theoretical silica content 20 wt.-%).

The screw speed was fixed at 25 rpm. The heating temperature was set from 90 to 130°C (as reported in Figure 1). The condensation by-products and excess water are extracted by degassing hole near to the end of the barrel at atmospheric conditions.

The same machine with the same parameters was used to melt mix EVA with a conventional silica powder. A master-batch with 20 wt.-% of silica was produced and used in the second extrusion process as substitute of the sol-gel silica to have a reference

obtained in the same conditions.

To provide a suitable mixing of sol-gel solution (TEOS/Water/Ethanol/catalyst) or preformed silica powder into the polymer melt, the screw features sets of transport (T), kneading (K) and counter conveying (R) elements as reported in Figure 1 were used. The kneading elements are maintained to mix and disperse silica particles, which might occur during processing, while reverse element to increase the residence time (to around 2-2.5 minutes) to allow the sol-gel reaction to goes on. The low temperature profile was chosen to avoid a rapid water and ethanol evaporation in the hopper and the first stages of the screw.

2.3.3. Step II: Melt mixing of the two master-batches (EVA-FR + EVA-silica)

The master-batch with FR and the second master-batch with silica were finally mixed in a second extrusion process to obtain the final compositions of 55 wt.-% of FR and 5 wt.-% of silica. The extruder used was the CTE35 with the same parameter already reported for the EVA with FR mixing process. The different formulations studied are listed in Table 1.

Table 1. EVA-based final formulations [wt.-%]

Sample	EVA	ATH	HM	Sol-Gel	SiO_2
EVA	100	/	/	/	/
EVA60ATH	40	60	/	/	/
EVA55ATH5Si	40	55	/	/	5
EVA55ATH5Sol-gel	40	55	/	5	/
EVA60HM	40	/	60	/	/
EVA55HM5Si	40	/	55	/	5
EVA55HM5Sol-gel	40	/	55	5	/

2.4. Test specimen production

The samples for cone tests (100x100x3 mm^3 specimens, respectively) were prepared by using a hot compression moulding press QLB-350×350×2 from Shanghai first rubber machinery works, the People's Republic of China. The moulding time was 10 minutes with a pressure of 10-12 MPa and a temperature of 150-170°C.

2.5. Characterization techniques.

2.5.1. Thermogravimetry

Thermogravimetric analyses (TGA) were carried in nitrogen from 50 to 700°C with a heating rate of 50°C/min, using a TA Discovery thermo balance (TA Instruments) (experimental error: ±0.1 wt.-%, ±1°C). The samples (ca. 10 mg) were placed in open platinum pans and fluxed with nitrogen (gas flow: 25 mL/min). $T_{onset5\%}$ (temperature, at which 5% weight loss occurs), T_{max} (temperature, at which maximum weight loss rate is achieved) and the mass of the final residues at 700°C were evaluated.

A customized program was used for simulating the heat treatment on sol-gel solution during the extrusion process and discussed later.

The gases evolved during the TGA analysis were transferred with Redshift transfer line kept at 280 °C with a gas flux of 65 ml/min to make sure that every component evolved in the TGA is transported to the IR apparatus. The Fourier Transform Infrared Spectroscopy (FTIR) was recorded every 6 s using a Elmer Spectrum Two instrument.

2.5.2. NMR

Solid-state NMR spectra were acquired by using a Bruker Avance III 500 spectrometer with a wide-bore 11.7 T magnet with operational frequencies for ^{1}H and ^{29}Si of 500.13

and 99.35 MHz, respectively. Either a 4 mm triple-resonance or a 7 mm double-resonance probe with magic-angle spinning (MAS) was employed in all experiments. The samples were packed on a zirconia rotor and spun at a MAS rate of 5-10 kHz. Quantitative ^{29}Si MAS NMR data were recorded under ^{1}H decoupling conditions with the radio-frequency field of 42 kHz for $\pi/2$ pulse. For the ^{29}Si Cross Polarization (CP) MAS experiments, the RF fields of 55 and 28 kHz were used for initial proton excitation and decoupling, respectively. During the CP period the ^{1}H RF field was ramped using 100 increments, whereas the ^{29}Si RF fields were maintained at a constant level. During the acquisition, the protons are decoupled from the silicons by using a two-pulse phase-modulated (TPPM) decoupling scheme. A moderate ramped RF field of 62 kHz was used for spin locking, while the silicon RF field was matched to obtain optimal signal and the CP contact time of 2 ms was used. The relaxation delay between accumulations was 3 and 120 minutes for CPMAS and MAS experiments, respectively. All chemical shifts are reported on the δ scale and were externally referenced to tetramethylsilane (TMS) at 0 ppm.

2.5.3. Limiting oxygen index (LOI)

The LOI values were measured using FTA II Instrument (Stanton Redcroft, Polymer Laboratory, UK) on the specimens of 120x 6x4 mm^3 according to the standard oxygen index test ASTM D2863.

2.5.4. UL-94 test

The UL-94 vertical burning tests were carried out using a Ul94-x test Chamber from Motis fire technology Co., Ltd (China) on the sheets of 127x12x3 mm^3 according to the

standard UL-94 test ASTM D635.

2.5.5. Cone calorimeter

Cone calorimeter tests (Fire Testing Technology, FTT, UK) were performed according to the ISO 5660 standard on 100x100x3 mm^3 specimens. The samples were wrapped in aluminium to avoid losing matter and irradiated in horizontal configuration under a 35kW/m^2 heat flux. For each formulation, the test was repeated three times and an experimental error was calculated as standard deviation for all the measured parameters. The reported data are average of the three repeated measurements. Time to Ignition (TTI, s), Total Heat Release (THR, MJ/m^2), peak of Heat Release Rate (PHRR, kW/m^2) and Total Smoke Release (TSR, m^2/m^2) were evaluated.

Fire Growth Rate index (FIGRA) (kW/m^2s) was calculated by dividing the HRR peak by the time when this peak was measured (TTP). FIGRA is often used to predict whether a material can easily develop drastic combustion after ignition. Therefore, the smallest FIGRA value, the better is the fire retardance.

Prior to the combustion tests, all the samples were conditioned at 23±1°C and 50% RH, in a climate-controlled chamber for 3 days.

Results and discussion

3.1. Silica from sol-gel process characterizations (Melt mixing step Ib)

In order to simulate and analyse the reactions occurring in the silica pre-gel during the extrusion process, a TGA with a customized program was used. Such TGA starts at room temperature and is raised to the extrusion temperature of 130°C in 3 minutes. This time is

comparable to the residence of the material inside the extruder when the silica network should be formed. After that, an isotherm of 120 minutes is set to check the material stability and possible evolutions over time. After the isotherm, a temperature ramp at 10°C/min up to 800°C was added to evaluate the subsequent evolutions of the formed silica network. The weight loss curve as a function of time is shown in the Figure 2a.

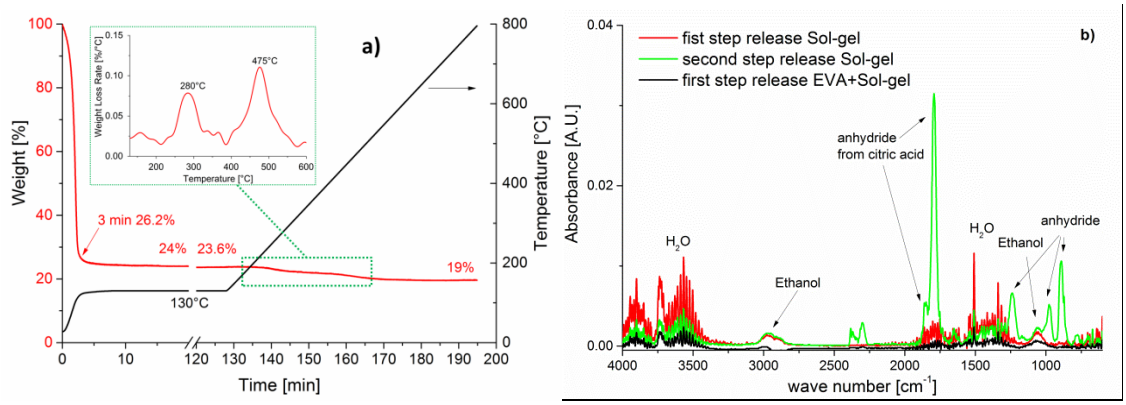

Figure 2. TGA analysis on pre-gel (a); FTIR spectra of gases evolved from TGA-FTIR at time corresponding to the greater weight losses of sol-gel (b).

The pre-gel loses almost 74% of the original weight in the first 3 minutes. This loss is due to the reaction of condensation that releases ethanol and water from the original TEOS/water/ethanol/citric acid solution. If a complete conversion from TEOS to SiO_2 take place, the residual weight should be 18%. Therefore a perfect silica lattice is not reached but only a network where reactive sites are still present. The structure formed is stable over time and only 2.2% of weight in the next two hours of isotherm is lost. Realistically, at the end of the extrusion process, the silica network still has sites available to react as shown in the Figure 3. In the final heating ramp, the silica structure is completed and the residue definitively decreases to 19% with two main weight losses centred at 280°C and 475°C. The final residue is not exactly 18% because probably in the

initial 3 h aging time there was evaporation in the solution (water and ethanol) that is not accounted in the TGA experiment.

FTIR analysis was used to characterize the gases evolved during the TGA in the temperature ramp step. The FTIR spectra registered at time corresponding to the two main weight losses are shown in the Figure 2b. The first weight loss presents a release of water and ethanol. A typical anhydride spectrum, due to the transformation of the citric acid, is observed in the second weight loss at higher temperature. However, the water and ethanol peaks are still present.

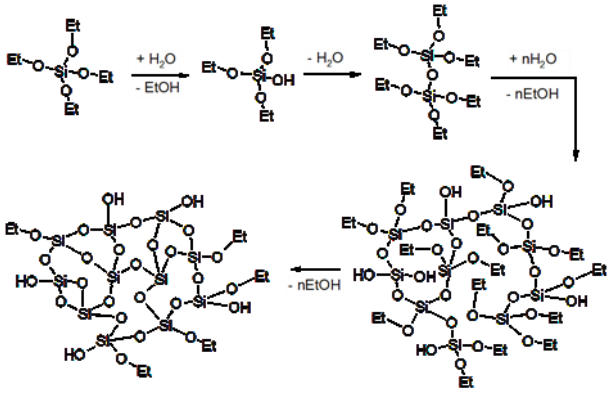

Figure 3 Reaction scheme of growing silica network.

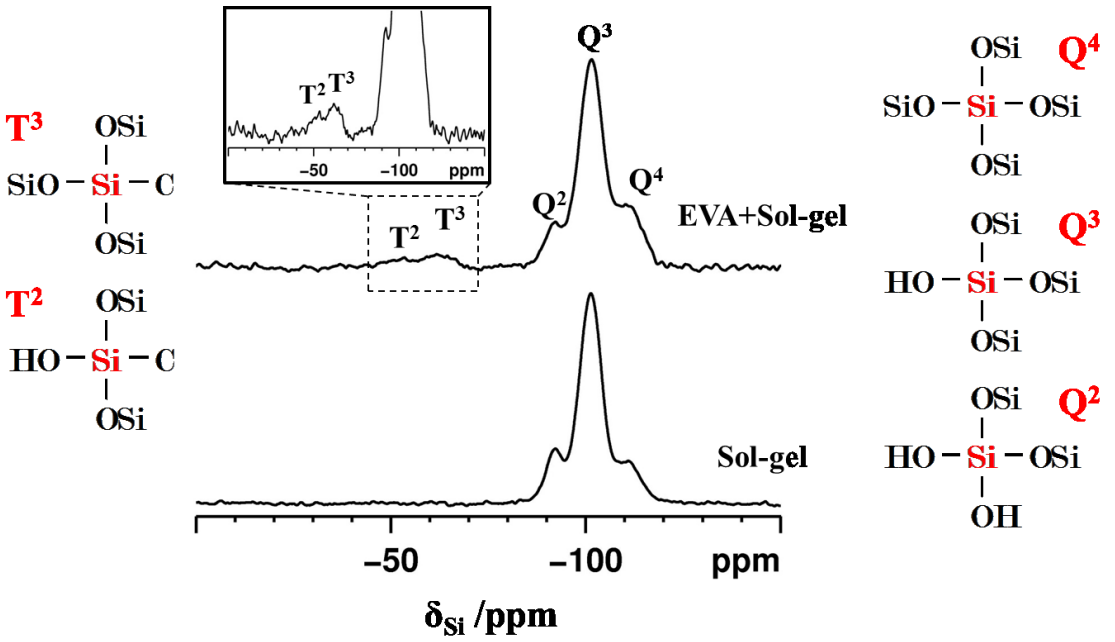

Figure 4: ^{29}Si CPMAS NMR spectra of samples recorded at a MAS rate of 10kHz and a cross-polarization contact time of 2 ms. Inset shows the zoomed spectra of sample EVA+Sol-gel.

^{29}Si NMR studies have been carried out in order to understand the fundamental silicon atom connectivity and structural pattern in these materials. In the first step, the sol-gel silica synthesis method and its compatibility with EVA extrusion process are evaluated. The hydrolysis-condensation process of TEOS was either conducted in the presence of EVA in an extruder or in the absence of EVA outside the extruder. The ^{29}Si CPMAS NMR spectra of samples recorded at a MAS spin rate of 10 kHz and a cross-polarization contact time of 2 ms are shown in Figure 4. The foundation of a CPMAS NMR experiment lies in the through-space magnetization transfer between ^{1}H and ^{29}Si via hetero-nuclear dipolar couplings. Consequently, ^{29}Si species in close proximities to proton nuclei, such as surface species, will have enhanced signal intensity. However, silicon species in the bulk, such as Q^4 units, will have a weakened intensity in the spectra.

Both samples showed resonances at around -110, -100 and -90 ppm due to Q^4 ($(SiO)_4$**Si**), Q^3 ($(SiO)_3$**Si**(OH)) and Q^2 ($(SiO)_2$**Si**$(OH)_2$) silicon network sites, respectively [31].

Although the CPMAS experiment is not quantitative, the relative ratio of populations of the partially condensed (Q^3 and Q^2) and fully condensed (Q^4) silicon sites, $(Q^3+Q^2)/Q^4$, gives an estimation of the degree of condensation in these silica networks. There is a difference in the ratio detected between samples, i.e., sol-gel sample with a value 7.3 and extruded Eva+Sol-gel with 4.4. The observed decrease in the estimated ratio is attributed to the higher rate of silica network condensation during extrusion process. However, for a preformed silica sample (for example, fumed silica or AEROSIL), this ratio would be an order smaller than the values reported here for sol-gel silica [32] [33]. Therefore, it can be presumed that the silica prepared through sol-gel method leads to highly uncondensed network than a preformed silica.

On the other hand, additional signals due to T^3 ($(SiO)_3$**Si**C) and T^2 ($(SiO)_2$**Si**C(OH)) silicon sites were detected at around -63 and -53 ppm, respectively, in the extruded sample (EVA+Sol-gel) as highlighted in Figure 4, inset. These resonances indicate the formation of Si-C bond during the extrusion process resulting in an organosilane based substructures within the silica networks. The Si–C bond formation (confirmed by the appearance of T^3 and T^2 peaks) and extended silica network condensation during extrusion process is a clear indication of the complete miscibility between EVA and sol-gel silica particles.

In order to investigate if the presence of silica changes the degradation behaviour of EVA and the production of volatile gases, the FTIR spectra were registered during the TGA and reported in the Figure 5.

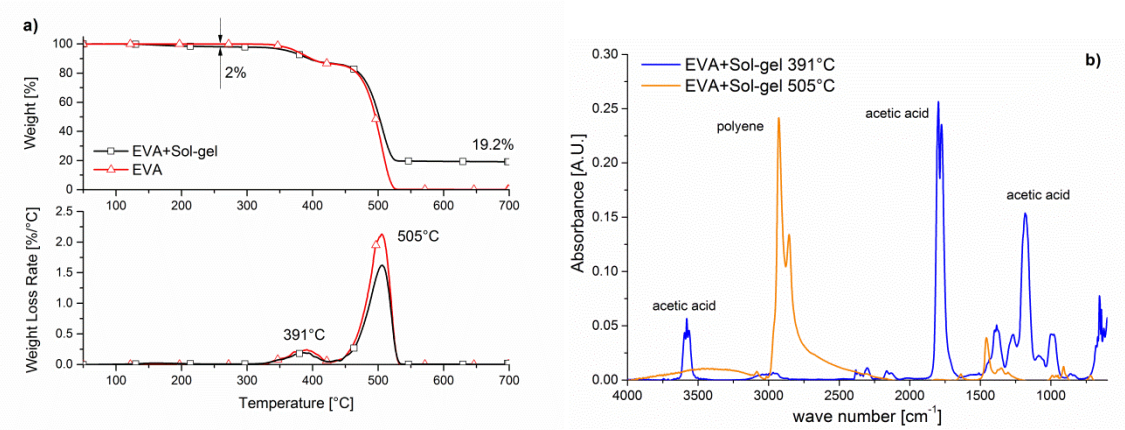

Figure 5. TGA and dTG/dT of EVA and EVA+Sol-gel (a) and FTIR spectra of gases evolved from TGA at the main weight loss rates of EVA+Sol-gel (b).

The degradation of the neat EVA occurs in two main steps Figure 5a. The first one at ca. 390 °C corresponds to the acetic acid release from EVA while the second degradation step occurs between 450 and 550°C and corresponds to the complete degradation of EVA. The presence of the siliceous structure does not modify the degradation of the neat EVA (see Figure 5a) and the evolving gases are exactly the same for both samples (only EVA+Sol-gel is reported in Figure 5b). The 2% weight loss highlighted in the Figure 5a before the 300°C, is identified by FTIR in water and ethanol, the two secondary products of the silica network production.

The final residue in the TGA analysis for EVA+Sol-gel is 19.2 %, in accordance with what was expected for the melt mixing in the step I.

3.2. Sol-gel silica in FR composites characterizations (Melt mixing step II)

The reactivity of sol-gel silica with the flame retardants, during the second melt mixing step, were investigated by employing combined ^{29}Si MAS NMR and TGA-FTIR

techniques. Furthermore, the state of silica network and the nature and concentration of silica surface reactive sites were estimated as they may play a critical role in subsequent fire tests.

The behaviour of the EVA based composites prepared using fire retardant HM and the two kinds of silica as co-filler were evaluated using ^{29}Si MAS NMR analysis (Figure 6). The poor signal to noise ratio of the spectra is due to the low amount of silica in these composite formulations. Since the amount of protons in a fire residue sample would be much lower, the ^{29}Si CPMAS experiment, which relay on the hetero-nuclear dipolar couplings between ^{1}H and ^{29}Si, would be futile. Therefore, ^{29}Si MAS NMR data has been recorded. Preformed silica based composite (EVA55HM5Si) showed a broad peak centred at around -110 ppm and is predominantly due to Q^4 silicon sites. The absence of Q^3 and Q^2 silicon sites confirms the fact that preformed silica is in a highly condensed network state. Similarly, ^{29}Si MAS NMR analysis of EVA composite based on sol-gel silica are presented in Figure 6 (EVA55HM5Sol-gel). Contrary to the preformed silica based sample, composites prepared using sol-gel silica showed resonances due to Q^3 Si sites, in addition to Q^4 sites. As the ^{29}Si MAS NMR spectra are quantitative, the relative ratio of Q^3/Q^4 clearly demonstrates a significant quantity of partially condensed silicon sites in sol-gel based composite. It is further suggested that the overall silica network structure in the composites vary according to the source of silica (preformed or sol-gel based) and the extrusion process. Furthermore, the sol-gel derived silica showed chemical interaction with EVA through Si-C bond formations in the composites.

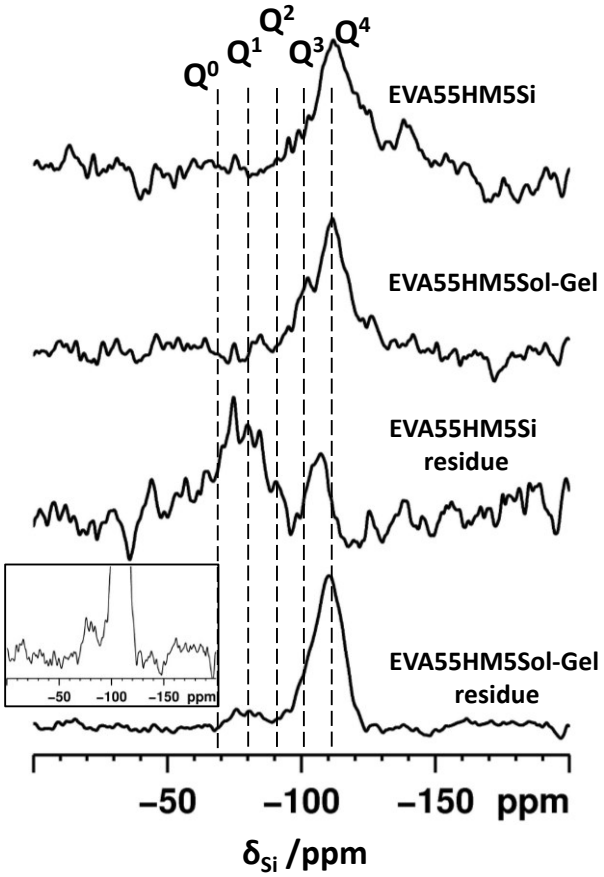

Figure 6: ***[29]Si MAS NMR spectra of samples recorded at a MAS rate of 5kHz and proton decoupling. Inset shows the zoomed spectra.***

Figure 7 shows the mass loss rate versus the temperature measured using TGA for all studied formulations and neat FRs and **Table 2** displays the main TGA data.

ATH has an endothermic loss of approximately 34% by mass of water as reported in the literature [34]. On the other hand, it is known that the decomposition of HM begins to occur at about 220°C and progresses through four mass losses at 275, 464, 520 and 661°C [34]. These losses are initially due to water of crystallization, followed by the hydroxide and carbonate decomposition, respectively [34]. These degradation temperatures are comparable to those found for the neat hydromagnesite reported in **Table 2**.

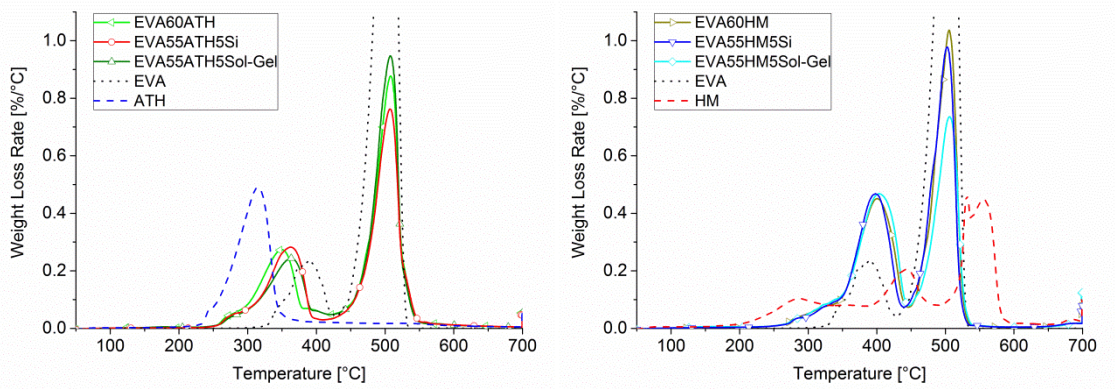

Figure 7. dTG/dT curves of studied EVA composites in nitrogen: ATH-based in (a) and HM-based in (b).

Table 2.TGA data of EVA-based composites in N_2

Sample Nitrogen	$T_{onset5\%}$ [℃]	T_{max1} [℃]	T_{max2} [℃]	700℃ experimental residue [%]	700℃ calculated residue [%]
EVA	375	391	505	0.1	-
ATH	276	314	-	65.7	-
EVA60ATH	320	349	508	40.2	39.4
EVA55ATH5Si	328	362	507	39.5	41.1
EVA55ATH5Sol-gel	328	363	508	44.1	41.1
HM	279	287	444-531-556	45.1	-
EVA60HM	343	400	505	26.4	27.1
EVA55HM5Si	345	398	503	29.0	29.8
EVA55HM5Sol-gel	338	404	506	32.9	29.8

The degradation of the composites occurs in two main steps exactly as previously reported for the EVA or EVA+Sol-gel. However, some changes in the weight loss rate are observed.

ATH causes the composite to have a first weight loss peak (T_{max1}) anticipated (-42°C) with respect to the one of the neat EVA while HM has the opposite effect (+9°C) (Table 2). Conversely, the second degradation step (T_{max2} in Table 2) remains essentially unchanged for all the samples. As far as the $T_{onset5\%}$ is concerned (Table 2), the presence of the fillers gave an anticipation of the weight loss start. This fact is probably due to the release of water from the fillers, and to confirm such hypothesis the FTIR on evolved gases has been performed.

The final residue of FR composites allows checking the true filler content. Indeed, considering the final weight for ATH and HM as 65.7% and 45.1% [35], respectively, and the EVA residue insignificant, the formulation with 60wt.-% of ATH and HM should have a residue of 39.4% and 27.1% (700℃ calculated residue in Table 2), respectively. The data obtained from the TGA residues (experimental) are in good agreement with the expected calculated contents. By considering the other composites with FRs and silica, the calculated residue was carried out from the nominal compositions reported in Table 1 and considering the weight loss due to the preformed or in situ silica as null. It is evident how the use of preformed silica generates a residue slightly lower (approximately 1%) than that calculated one while the use of silica from sol-gel induced a bit of additional carbonaceous char (approximately 3%) both in the formulation with ATH or with HM. This increase in the residue is an excellent signal for the possible barrier effect during the combustion of the composite.

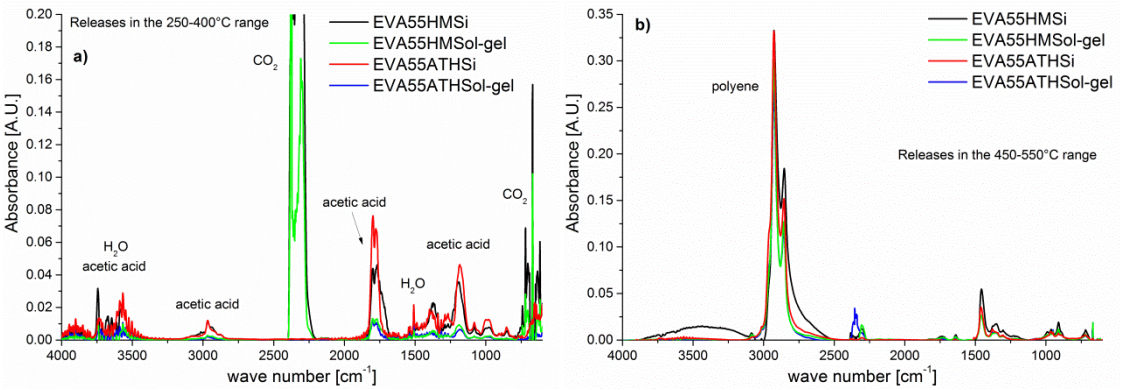

Figure 8. FTIR spectra of gases evolved from TGA: in the first degradation step 250-400°C (a) and in the second degradation step 450-550°C (b).

Figure 8a shows the FTIR spectra of gases evolved at T_{max1} which are characteristic of the whole first part of degradation from 250 to 400°C. The acetic acid release is derived from EVA degradation while the water release from ATH or HM. Furthermore, in the samples with HM there is also an intense release of CO_2 already at 320°C. Thus, once the fillers and the EVA are combined in the composite, the degradation kinetics of EVA as well as the water and CO_2 release from FRs are modified.

The second degradation step occurs between 450 and 550°C and corresponds to the complete degradation of EVA as visible in Figure 8b. In this case there is no obvious difference between the composite materials (Figure 8b) and the neat EVA (Figure 5b).

Finally, the partial substitution of FRs with silica does not modify the reported behaviour with not substantial differences between preformed silica and sol-gel silica (Figure 8b).

3.3. Fire retardant properties

3.3.1. Flammability (LOI and UL94)

The LOI and UL-94 tests are widely used to evaluate FR properties of materials and to

screen FR formulations. **Table 3** lists the related LOI and UL-94 data obtained from different loading of FR and silica from the two origins. It can be seen from **Table 3** that the LOI value of sample containing 60 wt.% of ATH or HM increases rapidly to 33 and 28.1 from 20.5 of unfilled EVA sample.

The LOI values of samples with Si as co-additive increase to 37 and 29.1 for EVA55ATH5Si and EVA55HM5Si, respectively. Thus, the silica has a better synergistic contribution in the composite with ATH. Conversely, the LOI value of sample with ATH and sol-gel as co-additive decreases to 31.5. On the other hand, the sol-gel used together with HM rises the LOI value to 36.7. These results indicate a different synergistic effect of the two kind of silica used. However, preformed SiO_2 with ATH or sol-gel silica with HM synergistically increase the flame retardancy of EVA.

The results obtained from the UL-94 tests also show that all the samples with ATH reach the V-1 rating while a V-0 is reached only by EVA55HM5Sol-gel.

Table 3. LOI and UL 94 data of specimens with the thickness of 3.2mm

Sample	LOI	UL94	t1(s)	t2(s)	Cotton ignition	Melt dripping	Burning to clamp
EVA	20.5	No	-	-	Yes	Yes	Yes
EVA60ATH	33.0	V-1	0	35.0	No	No	No
EVA55ATH5Si	37.0	V-1	0	24.0	No	No	No
EVA55ATH5Sol-gel	31.5	V-1	0.9	13.0	No	No	No
EVA60HM	28.1	V-2	1.4	88.6	No	No	No
EVA55HM5Si	29.1	No	-	-	Yes	Yes	Yes
EVA55HM5Sol-gel	36.7	V-0	0	0	No	No	No

3.3.2. Combustion behaviour (cone calorimeter test)

The HRR measured by cone calorimeter is a very important parameter as the HRR peak value is used to express the intensity of a fire. The changes of HRR as a function of burning time for different samples are shown in Figure 9. Furthermore, Table 4 summarizes all the main data measured using cone calorimeter at 35 kW/m^2.

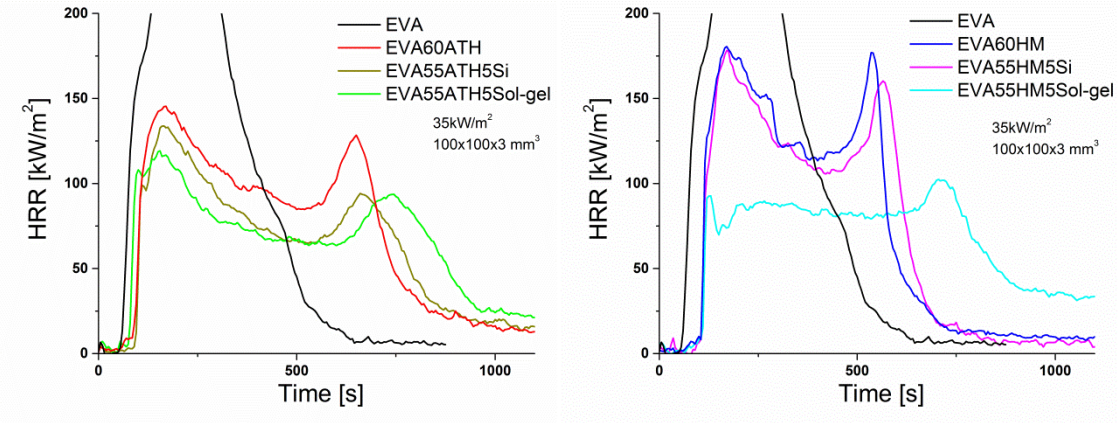

Figure 9. HRR curves from cone calorimeter tests at 35 kW/m^2

Table 4. Cone calorimeter data of EVA and composites.

Sample	Mass [g]	TTI [s]	pkHRR [kW/m^2]	THR [MJ/m^2]	TSR [m^2/m^2]	TTP [s]	FIGRA [kW/m^{2}s]
EVA	27.1	54±4	710.6±9.6	104.3±1.1	1077±119	215±5	3.30
EVA60ATH	46.6	91±1	144.2±1.3	75.6±2.0	436±39	167±3	0.86
EVA60HM	47.0	105±1	180.5±2.0	75.0±2.0	575±40	170±3	1.06
EVA55ATH5Si	47.7	92±1	135.0±1.2	70.7±2.3	391±42	162±3	0.83
EVA55HM5Si	45.5	94±10	179.8±1.5	73.4±0.4	629±39	167±3	1.07
EVA55ATH5Sol-gel	46.8	78±2	117.1±2.1	70.8±1.9	163±27	165±10	0.71
EVA55HM5Sol-gel	47.9	104±1	97.2±5.2	67.4±6.7	157±55	420±403	0.23

As it is known from the literature, the addition of aluminium hydroxide or hydromagnesite leads to a significant lowering of the HRR [10] [36] [9]. The HRR plot of FR samples in Figure 9 shows two separate peaks during burning as already reported in the literature [17]. This fact indicates the ability of the FR to form a protecting shield after the first HRR peak, that, unfortunately, cracks and allows the burning of the specimen through the thickness, giving rise to a second HRR peak [17, 37]. Anyhow, the highest peak (usually the first one) is considerably reduced from 710 to 144 and 180 kW/m^2 for ATH and HM composites, respectively. The HRR curves of the samples with or without silica were practically overlapped, in agreement with the results of Sonnier et al. [10] who observed that the incorporation of Sidistar® T-120 from ELKEM (a commercial name of silica) does not greatly modify the HRR peak of EVA/ATH composites.Conversely to preformed silica, the sol-gel silica reveals some important and significant changes in the combustion behaviour. Firstly, the peak of HRR is reduced with respect to preformed silica (18 kW/m^2 for ATH and 82 kW/m^2 for HM). Furthermore, the double peak feature is mitigated, especially for the EVA55HM5Sol-gel sample and the second peak is drastically delayed over time.

Table 4 also lists the FIGRA values of the studied samples (PHRR/TTP); the smaller FIGRA value, the better is the fire resistance. It can be seen that FR considerably decrease this value from 3.3 to 0.86 and 1.06 kW/m^{2}s for ATH and HM, respectively. Thus, the better result is reached with ATH with respect to HM. Preformed silica substantially never change this trend while the sol-gel silica reveals the best results for both ATH (0.71 kW/m^{2}s) and HM (0.23 kW/m^{2}s) formulations, with the best absolute result achieved with EVA55HM5Sol-gel.

Finally, the TSR was investigated. EVA has a high production of smoke 1077 m^2/m^2. The

FR reduced this value at around the half. Preformed silica does not substantially affect this parameter while the sol-gel silica enormously reduces the TSR to around 150 m^2/m^2 in both FRs formulations, around 15% of the neat EVA value and 25-40% of the corresponding preformed silica formulations.

Schartel and Schmaucks have tested the use of layered silicate (LS) together with fine spherical SiO_2 ($sSiO_2$) particles to flame-retard three different polymers without using a "real" flame retardant [38]. They reported a great enhancement in the protective layer effect in PP, PA 6, and PA 11 when LS and $sSiO_2$ were combined. This efficient protection is controlled mainly by the residue properties, in particular by the closed appearance of the surface correlated quite strongly with the protective properties and not by the amount of the residual layer [38]. The main effect proposed was the introduction of a residual layer working as heat shield.

Following this principle, the behavior during the cone calorimeter tests and the final residue were deeply investigated in the subsequent paragraphs.

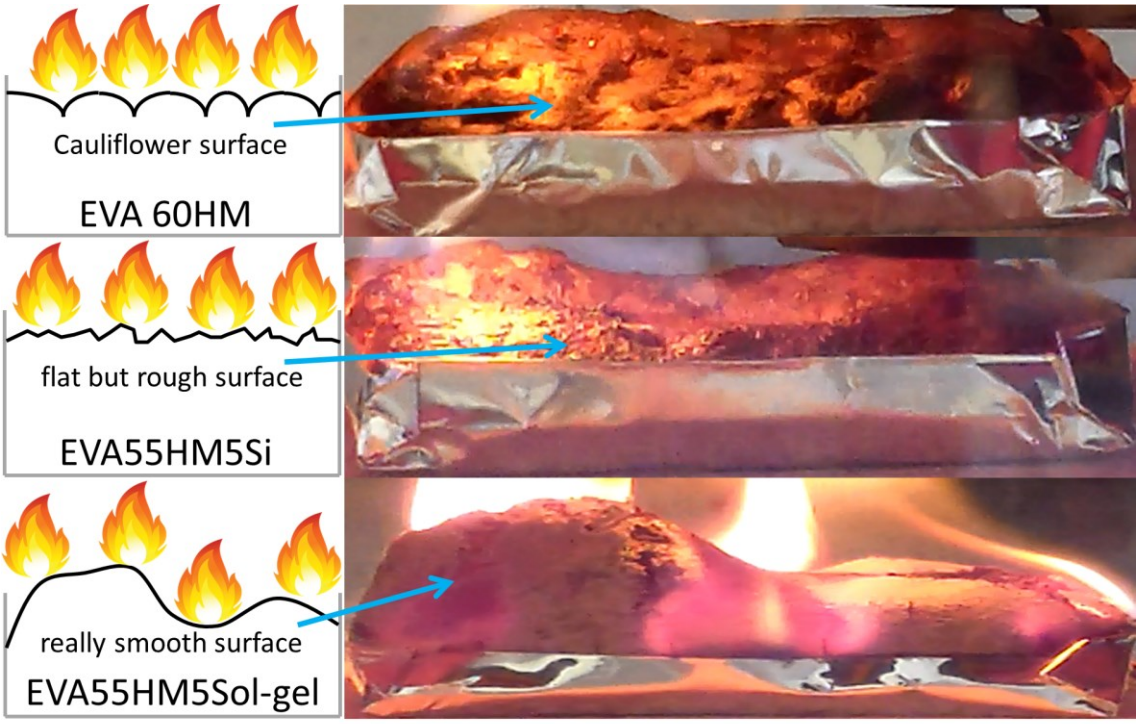

Figure 10. Images taken during the cone calorimeter tests after the ignition of EVA60HM, EVA55HM5Si and EVA55HM5Sol-gel.

In particular following the behavior of the HM-based samples, in the first pre-ignition phase the sample releases gases due to the degradation of the polymer and the FR. These gases increase over time until reaching the critical condition that gave the flame spread. At this point the surface of the samples is expanded with different layouts (Figure 10): it is similar to cauliflower for the neat HM, more flat but still rough for the formulations with preformed silica and very expanded and really smooth with sol-gel silica (Figure 10). In the case of ATH-based materials a similar trend was observed except for the EVA55ATH5Sol-gel in which the surface is still rough and not compact.

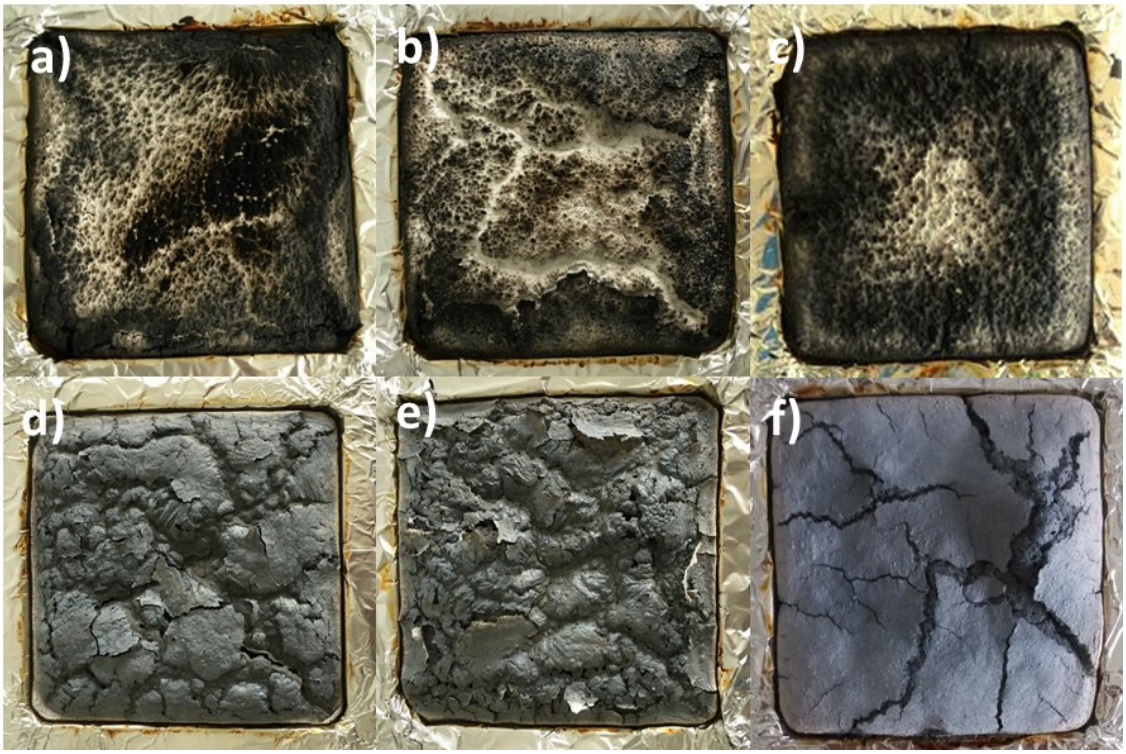

Figure 11. Cone residues of a) EVA60ATH, b) EVA55ATH5Si, c) EVA55ATH5Sol-gel, d) EVA60HM, e) EVA55HM5Si, f) EVA55HM5Sol-gel.

Figure 11 shows the residues obtained at the end of the cone calorimeter tests. All samples are expanded and partially reduced during cone calorimetry tests. On one hand, the preformed silica seems to produce a greater fragmentation of the upper surface (compare Figure 11a-b and Figure 11d-e) while the silica from the sol-gel promote the consistence and continuity of the char that protect the underlying material (compare Figure 11a-c and Figure 11d-f).

It is of note that the cracks in the EVA55HM5Sol-gel (Figure 11f) are not formed at the end of the cone test, but only once the structure cools. This continuous layer is a result of a better residue cohesion generated by the 3D network created by the sol-gel silica. All the reported improved fire behaviours obtained with sol-gel silica, are due to a physical action promoted by the three-dimensional silica lattice well dispersed within the polymer

matrix. This hypothesis is supported by images of the residue in Figure 11 and from the observations made by ^{29}Si CPMAS and/or MAS NMR data concerning the presence of chemical Si-C bonds (Figure 4), and the formation of silica lattice (Figure 6).

The ^{29}Si MAS NMR spectrum recorded on the preformed silica based residue sample, (EVA55HM5Si residue) after burning (Figure 6) showed a dramatic decrease in the Q^4 intensity, instead a broad peak appeared in the range -70 to -95 ppm. Silicate units as oligomers (dimers, trimers, tetramers and so on) or chains generally appear in this chemical shift range. Further considerations helped us to assign the broad peak in the range -70 to -95 ppm to magnesium silicate [39] [40]. Thus, preformed silica based composites lead also to the formation of a considerable quantity of magnesium silicate upon burning.

In the sol-gel based composite residue sample (EVA55HM5Sol-gel residue), most of the Q^3 sites were converted to fully condensed Q^4 units during the combustion as shown in the spectrum in Figure 6, traces of magnesium silicate can be identified. Previous works [41] [42] on char residues has demonstrated that high temperature treatment and the presence of other species in the FR formulations leads to modification of silicate frameworks and condensed silica were formed. Contrary to these reported studies that not evidenced mixed silicates, in our one a very small fraction of magnesium silicate was formed upon burning as evidenced by the broad peak detected in the range -70 to -95 ppm with very low intensity (Figure 6, inset). Further XRD analyses on EVA55HM5Si and EVA55HM5Sol-gel residues obtained from the cone calorimeter are reported in the Supporting Information as Figure S1. The spectra revealed the presence of crystalline MgO, $CaCo_3$, Mg_2SiO_4 and SiO_2 in a non-substantially different amounts for the two residues. Combining this result with the data obtained from the ssNMR, it is assumed that

the higher quantity of magnesium silicate found in EVA55HM5Si residue is due to the amorphous phase.

As previously reported [38], the main fire retardant effect related to the use of silica as co-filler is the residual layer that work as heat shield. The shield does not appear to be strong enough in the case of preformed silica. Conversely, the organosilane based silica network substructures shield EVA during fire and grow into pure silica 3D structures. It is thus demonstrated that the innovative *in-situ* extrusion approach of composite preparation, using sol-gel silica as co-filler, leads to better flame retardant properties with reduced heat release and reduced smoke production.

4. Conclusions

More efficient EVA-based flame retarded composites have been successfully prepared by replacing part of the aluminium hydroxide (ATH) or hydromagnesite (HM) with silica formed in-situ during the extrusion process (bottom-up approach), as compared with samples added with preformed silica (top-down approach). The ^{29}Si NMR spectroscopy shows that the sol-gel silica lattice formed during the extrusion is not completely condensed and, furthermore, it reacts with the polymer forming an organic-inorganic network. Furthermore, it has proved that this technique is a well suited method for the efficient characterization of framework state of different silica produced (bottom-up or top-down process).

Thanks to the detailed characterization techniques of thermogravimetry connected to the identification by FTIR of the evolved gases, it has been shown that both preformed and in-situ prepared silica does not lead to any change in the polymer degradation mechanism. However, through the innovative in-situ extrusion approach, better flame retardant properties are reached with respect to the use of only hydrated FRs, such as the best UL94

classification (V-0), reduced peak of heat release (-46%) and smoke production (-72%) for the EVA55HM5Sol-gel sample.

The 3D condensed silica network structure, that is dominant in the in-situ formed silica based composite, plays the key role in the formation of consistent and compact residue able to shield the underlay material. On the other hand, the interaction of the preformed silica with the formation of more magnesium silicate and the different inorganic microstructure, leads to a brittle char and to a lower quality shield.

Acknowledgements

Supported by the International Science and Technology Cooperation Program of China (No. 2014DFA52900)

References

[1] Henderson AM. Ethylene-vinyl acetate (EVA) copolymers: a general review. IEEE Electrical Insulation Magazine. 1993;9:30-8.
[2] Hull TR, Price D, Liu Y, Wills CL, Brady J. An investigation into the decomposition and burning behaviour of Ethylene-vinyl acetate copolymer nanocomposite materials. Polymer Degradation and Stability. 2003;82:365-71.
[3] Laoutid F, Gaudon P, Taulemesse JM, Lopez Cuesta JM, Velasco JI, Piechaczyk A. Study of hydromagnesite and magnesium hydroxide based fire retardant systems for ethylene–vinyl acetate containing organo-modified montmorillonite. Polymer Degradation and Stability. 2006;91:3074-82.
[4] Cárdenas MÁ, Basurto FC, García-López D, Merino JC, Pastor JM. Mechanical and fire retardant properties of EVA/clay/ATH nanocomposites: effect of functionalization of organoclay nanofillers. Polymer Bulletin. 2013;70:2169-79.
[5] Cavodeau F, Otazaghine B, Sonnier R, Lopez-Cuesta J-M, Delaite C. Fire retardancy of ethylene-vinyl acetate composites – Evaluation of synergistic effects between ATH and diatomite fillers. Polymer Degradation and Stability. 2016;129:246-59.
[6] Dittrich B, Wartig K-A, Mülhaupt R, Schartel B. Flame-Retardancy Properties of Intumescent Ammonium Poly(Phosphate) and Mineral Filler Magnesium Hydroxide in Combination with Graphene. Polymers. 2014;6:2875-95.
[7] El Hage R, Viretto A, Sonnier R, Ferry L, Lopez-Cuesta J-M. Flame retardancy of ethylene vinyl acetate (EVA) using new aluminum-based fillers. Polymer Degradation and Stability. 2014;108:56-67.
[8] Rychlý J, Veselý K, Gal E, Kummer M, Jančář J, Rychla L. Use of thermal methods in the characterization of the high-temperature decomposition and ignition of polyolefins and EVA copolymers filled with Mg (OH) 2, Al (OH) 3 and CaCO 3. Polymer

Degradation and Stability. 1990;30:57-72.
[9] Haurie L, Fernández AI, Velasco JI, Chimenos JM, Lopez Cuesta J-M, Espiell F. Synthetic hydromagnesite as flame retardant. Evaluation of the flame behaviour in a polyethylene matrix. Polymer Degradation and Stability. 2006;91:989-94.
[10] Sonnier R, Viretto A, Dumazert L, Longerey M, Buonomo S, Gallard B, et al. Fire retardant benefits of combining aluminum hydroxide and silica in ethylene-vinyl acetate copolymer (EVA). Polymer Degradation and Stability. 2016;128:228-36.
[11] Oliveira M, Machado AV. Preparation and characterization of ethylene-vinyl acetate nanocomposites: enhanced flame retardant. Polymer International. 2013;62:1678-83.
[12] Jiao C, Wang Z, Ye Z, Hu Y, Fan W. Flame retardation of ethylene-vinyl acetate copolymer using nano magnesium hydroxide and nano hydrotalcite. Journal of fire sciences. 2006;24:47-64.
[13] Cross M, Cusack P, Hornsby P. Effects of tin additives on the flammability and smoke emission characteristics of halogen-free ethylene-vinyl acetate copolymer. Polymer degradation and stability. 2003;79:309-18.
[14] Bourbigot S, Le Bras M, Leeuwendal R, Shen KK, Schubert D. Recent advances in the use of zinc borates in flame retardancy of EVA. Polymer Degradation and Stability. 1999;64:419-25.
[15] Carpentier F, Bourbigot S, Le Bras M, Delobel R, Foulon M. Charring of fire retarded ethylene vinyl acetate copolymer—magnesium hydroxide/zinc borate formulations. Polymer Degradation and Stability. 2000;69:83-92.
[16] Durin-France A, Ferry L, Lopez Cuesta JM, Crespy A. Magnesium hydroxide/zinc borate/talc compositions as flame-retardants in EVA copolymer. Polymer International. 2000;49:1101-5.
[17] Fu M, Qu B. Synergistic flame retardant mechanism of fumed silica in ethylene-vinyl acetate/magnesium hydroxide blends. Polymer Degradation and Stability. 2004;85:633-9.
[18] Jiao CM, Chen XL. Synergistic flame retardant effect of cerium oxide in ethylene-vinyl acetate/aluminum hydroxide blends. Journal of applied polymer science. 2010;116:1889-93.
[19] Milea C, Bogatu C, Duta A. The influence of parameters in silica sol-gel process. Bulletin of TheTransilvania University of Brasov. 2011;4:53.
[20] Bounor-Legaré V, Cassagnau P. In situ synthesis of organic–inorganic hybrids or nanocomposites from sol–gel chemistry in molten polymers. Progress in Polymer Science. 2014;39:1473-97.
[21] Brinker CJ, Scherer GW. Sol-gel science: the physics and chemistry of sol-gel processing: Academic press; 2013.
[22] Dou Q, Zhu X, Peter K, Demco DE, Möller M, Melian C. Preparation of polypropylene/silica composites by in-situ sol–gel processing using hyperbranched polyethoxysiloxane. Journal of Sol-Gel Science and Technology. 2008;48:51-60.
[23] Prebe A. Different Routes for Synthesis of Poly (lactic Acid): Silicon-based Hybrid Organic-inorganic Nanomaterials and Nanocomposites: éditeur inconnu; 2010.
[24] Mougin B. Elaboration de matériaux nanocomposites polyamide 6, 6-silice par génération in situ de la charge inorganique au cours du procédé d'extrusion: Lyon 1; 2005.
[25] Liao H-T, Wu C-S. Organic–inorganic polymeric nanocomposites involving novel titanium tetraisopropylate in polyethylene–octene elastomer. Journal of Polymer Science Part B: Polymer Physics. 2004;42:4272-80.

[26] Wu CS. Synthesis of polyethylene-octene elastomer/SiO2-TiO2 nanocomposites via in situ polymerization: Properties and characterization of the hybrid. Journal of Polymer Science Part A: Polymer Chemistry. 2005;43:1690-701.
[27] Oliveira M, Nogueira R, Machado A. Synthesis of aluminium nanoparticles in a PP matrix during melt processing: Effect of the alkoxide organic chain. Reactive and Functional Polymers. 2012;72:703-12.
[28] Kluenker E, Faymonville J, Peter K, Moeller M, Hopmann C. Reactive extrusion processing of polypropylene/SiO 2 nanocomposites by in situ synthesis of the nanofillers: Experiments and properties. Polymer. 2014;55:5370-80.
[29] Yeh J-T, Chai W-L, Wu C-S. Study on the Preparation and Characterization of Biodegradable Polylactide/SiO2–TiO2 Hybrids. Polymer-Plastics Technology and Engineering. 2008;47:887-94.
[30] Bonnet J, Bounor-Legaré V, Boisson F, Melis F, Camino G, Cassagnau P. Phosphorus based organic–inorganic hybrid materials prepared by reactive processing for EVA fire retardancy. Polymer Degradation and Stability. 2012;97:513-22.
[31] Paul G, Bisio C, Braschi I, Cossi M, Gatti G, Gianotti E, et al. Combined solid-state NMR, FT-IR and computational studies on layered and porous materials. Chemical Society Reviews. 2018;47:5684-739.
[32] Mijatovic J, Binder WH, Gruber H. Characterization of surface modified silica nanoparticles by 29 Si solid state NMR spectroscopy. Microchimica Acta. 2000;133:175-81.
[33] Liu CC, Maciel GE. The fumed silica surface: A study by NMR. Journal of the American Chemical Society. 1996;118:5103-19.
[34] Hollingbery L, Hull TR. The fire retardant behaviour of huntite and hydromagnesite–A review. Polymer degradation and stability. 2010;95:2213-25.
[35] Laoutid F, Ferry L, Leroy E, Lopez Cuesta JM. Intumescent mineral fire retardant systems in ethylene–vinyl acetate copolymer: Effect of silica particles on char cohesion. Polymer Degradation and Stability. 2006;91:2140-5.
[36] Hull TR, Witkowski A, Hollingbery L. Fire retardant action of mineral fillers. Polymer Degradation and Stability. 2011;96:1462-9.
[37] Le Bras M, Bourbigot S, Revel B. Comprehensive study of the degradation of an intumescent EVA-based material during combustion. Journal of materials science. 1999;34:5777-82.
[38] Schartel B, Schmaucks G. Flame retardancy synergism in polymers through different inert fillers' geometry. Polymer Engineering & Science. 2017;57:1099-109.
[39] Brew D, Glasser F. Synthesis and characterisation of magnesium silicate hydrate gels. Cement and Concrete Research. 2005;35:85-98.
[40] Lothenbach B, Nied D, L'Hôpital E, Achiedo G, Dauzères A. Magnesium and calcium silicate hydrates. Cement and Concrete Research. 2015;77:60-8.
[41] Hansupo N, Tricot G, Bellayer S, Roussel P, Samyn F, Duquesne S, et al. Getting a better insight into the chemistry of decomposition of complex flame retarded formulation: New insights using solid state NMR. Polymer Degradation and Stability. 2018;153:145-54.
[42] Karrasch A, Wawrzyn E, Schartel B, Jäger C. Solid-state NMR on thermal and fire residues of bisphenol A polycarbonate/silicone acrylate rubber/bisphenol A bis (diphenyl-phosphate)/(PC/SiR/BDP) and PC/SiR/BDP/zinc borate (PC/SiR/BDP/ZnB)–Part I: PC charring and the impact of BDP and ZnB. Polymer degradation and stability. 2010;95:2525-33.